18th AIAA/CEAS Aeroacoustics Conference (33rd AIAA Aeroacoustics Conference)
04 - 06 June 2012, Colorado Springs, CO

AIAA 2012-2249

Effects of initial shear-layer thickness on turbulent subsonic jets at moderate Reynolds numbers

Christophe Bogey[*], **Olivier Marsden**[†] and **Christophe Bailly**[‡]

Laboratoire de Mécanique des Fluides et d'Acoustique

UMR CNRS 5509, Ecole Centrale de Lyon

69134 Ecully, France

Large-Eddy Simulations of isothermal round jets at a Mach number of 0.9 are performed in order to investigate the influence of the nozzle-exit boundary-layer thickness on initially highly disturbed subsonic jets at moderate Reynolds numbers. The jets are originating from a pipe nozzle of radius r_0, and exhibit, at the exit section, peak disturbance levels of 9 per cent of the jet velocity, and mean velocity profiles similar to laminar boundary-layer profiles of thickness $\delta_0 = 0.09r_0$, $0.15r_0$, $0.25r_0$ or $0.42r_0$, yielding momentum thicknesses $\delta_\theta(0)$ between $0.012r_0$ and $0.05r_0$. Four jets at a diameter Reynolds number $\mathrm{Re}_D = 5 \times 10^4$, providing momentum-thickness Reynolds numbers $\mathrm{Re}_\theta = 304$, 486, 782 and 1288 depending on δ_0, are first considered. Four jets at Reynolds numbers $\mathrm{Re}_D = 8.3 \times 10^4$, 5×10^4, 3×10^4 and 1.8×10^4, with $\delta_0 = 0.09r_0$, $0.15r_0$, $0.25r_0$ and $0.42r_0$, respectively, giving $\mathrm{Re}_\theta \simeq 480$ in all cases, are then examined. The effects of δ_0/r_0 and Re_θ on the jet flow and sound fields can thus be distinguished. At a constant Re_D, thickening the initial shear layers mainly results in lower turbulence intensities in the mixing layers and weaker sound levels at all emission angles due to the variations of Re_θ. Different trends are therefore obtained at a nearly identical Re_θ. Increasing the ratio δ_0/r_0 in this case leads to a shorter potential core, higher centerline velocity fluctuations, and stronger noise in the downstream direction.

I. Introduction

The crucial role of the initial conditions in free shear flows has been well recognized for more than thirty years. The turbulent development and acoustic field of jets have in particular been been shown to depend on nozzle-exit parameters such as the Reynolds number, the mean velocity profile, the thickness and the shape factor of the boundary layer, and the disturbance level, just to mention a few important ones, as pointed out in the reference papers by Hussain[1] and Crighton.[2] These parameters are moreover likely to vary significantly from one experiment to another. This is notably the case for the initial shear-layer thickness δ_0 or momentum thickness $\delta_\theta(0)$. In two recent experimental studies on round jets of diameter D or radius r_0, for example, Morris & Zaman[3] measured $\delta_\theta(0) = 0.0013r_0$ in a jet at a Mach number M= 0.25 and at a diameter-based Reynolds number $\mathrm{Re}_D = 3 \times 10^5$, whereas Arakeri *et al.*[4] found $\delta_\theta(0) \simeq 0.04r_0$ in a jet at M= 0.9 and $\mathrm{Re}_D = 5 \times 10^5$.

The thickness of the nozzle-exit boundary layer in jets however appears to follow general trends. In initially laminar jets, it decreases with increasing Reynolds number following a $1/\mathrm{Re}_D^{1/2}$ proportionality law, which was predicted for instance by Becker & Massaro[10] based on simple boundary-layer concepts, and was verified experimentally by Crow & Champagne,[5] Zaman[6–8] and Deo,[9] among others. The constant of proportionality obviously depends on the nozzle geometry and contraction ratio. The influence of a constant-diameter tail-pipe attached to the downstream end of the nozzle was for example explored by Hasan & Hussain.[11] Recently, tests were performed using three nozzles of identical exit diameter, differing only in internal profile. The results obtained using the so-called ASME, cubic and conic nozzles have been

[*]CNRS Research Scientist, AIAA Member, christophe.bogey@ec-lyon.fr

[†]Assistant Professor at Ecole Centrale de Lyon, AIAA Member, olivier.marsden@ec-lyon.fr

[‡]Professor at Ecole Centrale de Lyon & Institut Universitaire de France, Senior AIAA Member, christophe.bailly@ec-lyon.fr

discussed by Viswanathan & Clark,[12] Harper-Bourne[13] and Zaman.[8] In the vicinity of the transition to turbulent upstream conditions, the exit boundary-layer thickness then sharply rises by a factor between 2 and 4 with respect to the initially laminar case. This jump is observed when the flow transition in the nozzle is forced by a tripping device as in Zaman,[6,7] Bridges & Hussain,[14] Raman *et al.*,[15] or Morris & Zaman,[3] as well as when it occurs naturally as in Zaman.[8] Finally, in initially turbulent jets, according to the latter author,[8] the nozzle-exit boundary-layer thickness decreases only marginally with the Reynolds number.

The effects of the initial shear-layer thickness in jets are unfortunately difficult to investigate experimentally, because it cannot usually be modified independently of the initial turbulence level. Furthermore, experiments are generally performed for jets with a fixed diameter, hence at a constant Reynolds number Re_D but at varying momentum-thickness-based Reynolds numbers Re_θ when the value of δ_0 is changed and the flow velocity remains the same. This was the case for instance in the work by Hussain & Zedan,[16] which dealt with axisymmetric mixing layers characterized initially by similar peak rms velocities $u'_e/u_j \simeq 6\%$ and different thicknesses yielding Reynolds numbers Re_θ between 184 and 349. The variations with the initial shear-layer thickness δ_0 obtained in this way can be expected to result from the modification of both the ratio δ_0/r_0 and the value of Re_θ, or, in other words, from both geometry and viscosity effects. The influence on linear instability waves of the two parameters above has been investigated theoretically by Michalke[17] and Cohen & Wygnanski[18] for the former, and by Morris[19,20] for the latter. It was found that increasing δ_0/r_0 or Re_θ generally leads to lower growth rates, but does not fundamentally alter the Strouhal number St_θ of maximum amplification, in agreement with the experimental data collected in Gutmark & Ho.[21] Nevertheless, the effects of the Reynolds number Re_θ are well known to be significant on turbulent mixing layers. As Re_θ increases, more fine-scale structures are observed, as clearly shown by the experiments of Brown & Roshko,[22] or by the simulations of Kleinman & Freund.[23] The shear layers also develop more slowly, with lower levels of velocity fluctuations, according to the calculations of Bogey *et al.*[24]

Given the issues outlined previously, it appears interesting to perform simulations in order to carefully investigate the effects of the initial shear-layer thickness on jets, refer for instance to the papers by Colonius & Lele,[25] Bailly & Bogey[26] and Wang *et al.*[27] reviewing the rapid progress in computation of jet noise. It can be noted that a number of numerical studies have already been conducted on this matter over the last twelve years. Stanley & Sarkar[28] and Bogey & Bailly[29] first examined plane and round jets without including a nozzle in the computational domain, for which hyperbolic-tangent velocity profiles were imposed at the inflow boundary. Kim & Choi[30] and Bogey & Bailly[31] later focused on round jets with fully laminar conditions downstream of a pipe nozzle. In the work of the latter authors, jets at a Mach number of 0.9 and at a Reynolds number $\mathrm{Re}_D = 10^5$, with an inlet boundary-layer thickness $\delta_0 = 0.025$, 0.05, 0.1 or 0.2, were considered. Shorter potential cores and higher centreline turbulence intensities were observed with increasing δ_0. In all cases, however, the shear-layer transitions were dominated by vortex rolling-ups and pairings, generating strong noise components.

The objective of the present work is now to investigate, for the first time to the best of our knowledge, the influence of the nozzle-exit boundary-layer thickness on the flow and acoustic fields of initially highly disturbed subsonic round jets. For this, Large-Eddy Simulations based on low-dissipation schemes and relaxation filtering as subgrid model are carried out. The jets are at a Mach number of 0.9, and at moderate Reynolds numbers Re_D between 1.8×10^4 and 8.3×10^4 to ensure the numerical accuracy of the LES using a 252 million point grid.[32,33] In the same way as in recent studies, devoted notably to the importance of the initial disturbance level[34] and of the Reynolds number,[24] a trip-like excitation is applied to the jet boundary layers in a pipe nozzle, in order to obtain, at the exit, peak turbulence intensities $u'_e/u_j = 9\%$, where u_j is the jet velocity, and mean velocity profiles similar to Blasius laminar profiles. Seven jet simulations are reported here. The first jet has a Reynolds number $\mathrm{Re}_D = 5\times10^4$ and a boundary-layer thickness $\delta_0 = 0.15r_0$, yielding $\delta_\theta(0) = 0.019r_0$ and $\mathrm{Re}_\theta = 486$ at the nozzle exit.[24] The next three jets are also at $\mathrm{Re}_D = 5 \times 10^4$, but they have thinner or thicker initial shear layers with respect to the first case. More precisely, values $\delta_0 = 0.09r_0$, $0.25r_0$ and $0.42r_0$ are chosen, leading to Re_θ around 300, 800 and 1300. The same ratios $\delta_0/r_0 = 0.09$, 0.25 and 0.42 are specified in the last three jets. The diameter Reynolds numbers are however set to $\mathrm{Re}_D = 8.3\times10^4$, 3×10^4 and 1.8×10^4, respectively, in order to maintain $\mathrm{Re}_\theta \simeq 480$. We should consequently be able to distinguish between the effects of δ_0/r_0 and Re_θ on the jet characteristics.

The paper is organized as follows. In section II, the main parameters of the jets and of the simulations are documented. In section III, the nozzle-exit flow conditions, and the aerodynamic and acoustic fields obtained for the four jets at $\mathrm{Re}_D = 5 \times 10^4$ are first presented. The results for the jets at $\mathrm{Re}_\theta \simeq 480$ are then shown. Finally, concluding remarks are provided in section IV.

II. Parameters

In this section, the jet inflow conditions are first presented. The numerical methods and parameters are then briefly reported. They are identical to those used in recent jet simulations, which have been thoroughly described in previous references.[24,31–34] The simulation of the jet at $\mathrm{Re}_D = 5 \times 10^4$ with a boundary-layer thickness $\delta_0 = 0.15 r_0$ considered in the present study was moreover performed for the first time and detailed in Bogey *et al.*[24] A great deal of information about the boundary-layer tripping procedure, the discretization quality and the LES reliability is also available in other papers.[32,33]

A. Jet definition

Seven isothermal round jets at a Mach number $\mathrm{M} = u_j/c_a = 0.9$ and at Reynolds numbers $\mathrm{Re}_D = u_j D/\nu$ over the range $1.8 \times 10^4 \leq \mathrm{Re}_D \leq 8.3 \times 10^4$, where c_a is the ambient speed of sound and ν is the kinematic molecular viscosity, are investigated. They originate at $z = 0$ from a pipe nozzle of radius r_0 and length $2r_0$, whose lips are $0.053 r_0$ thick. The ambient temperature and pressure are $T_a = 293$ K and $p_a = 10^5$ Pa. For all jets, an axial velocity profile, corresponding to a Blasius laminar boundary-layer profile of thickness δ_0, is imposed at the pipe inlet. Radial and azimuthal velocities are initially set to zero, pressure is set to p_a, and the temperature is determined by a Crocco-Busemann relation.

A trip-like forcing is applied to the jet boundary layers by adding random low-level vortical disturbances decorrelated in the azimuthal direction at $z = -r_0$ inside the pipe. The excitation magnitudes are empirically chosen in order to obtain, at the pipe exit, peak turbulence intensities u'_e/u_j around 9% as in the tripped subsonic jets of Zaman,[6,7] and mean velocity profiles in fair agreement with the Blasius laminar profiles introduced at the pipe inlet, which will be illustrated in sections III.A.1 and III.B.1. Pressure fluctuations of maximum amplitude 200 Pa random in both space and time are also added in the shear layers between $z = 0.25 r_0$ and $z = 4 r_0$ from $t = 0$ up to non-dimensional time $t = 12.5 r_0/u_j$, in order to speed up the initial transitory period.

As shown in tables 1 and 2, the four values of boundary-layer thickness $\delta_0 = 0.09 r_0$, $0.15 r_0$, $0.25 r_0$ and $0.42 r_0$ are considered. They will result in nozzle-exit momentum thicknesses over the range $0.012 r_0 \leq \delta_\theta(0) \leq 0.05 r_0$. The initial shear layers of the jets are therefore relatively thick. This is encountered in some experiments on tripped jets, such as those of Zaman[6,7] and Arakeri *et al.*,[4] in which $\delta_\theta(0) = 0.018 r_0$ and $\delta_\theta(0) \simeq 0.04 r_0$ were measured at $\mathrm{Re}_D \simeq 10^5$ and $\mathrm{Re}_D = 5 \times 10^5$, respectively. In a first step, jets at a constant $\mathrm{Re}_D = 5 \times 10^4$, hence at momentum-thickness Reynolds numbers $\mathrm{Re}_\theta = u_j \delta_\theta(0)/\nu$ between about 300 and 1300 depending on δ_0/r_0, are examined, refer to table 1. In a second step, conversely, the diameter Reynolds number of the jets varies in such a way that $\mathrm{Re}_\theta \simeq 480$ can be expected in all cases, as indicated in table 2.

Table 1. Inflow conditions for the jets at $\mathrm{Re}_D = 5 \times 10^4$: Mach and Reynolds numbers M and Re_D, inlet boundary-layer thickness δ, and intended Reynolds number Re_θ based on the nozzle-exit boundary-layer momentum thickness.

M	Re_D	δ_0/r_0	Re_θ
0.9	5×10^4	0.09	~ 300
0.9	5×10^4	0.15	~ 480
0.9	5×10^4	0.25	~ 800
0.9	5×10^4	0.42	~ 1300

Table 2. Inflow conditions for the jets at $\mathrm{Re}_\theta \simeq 480$: Mach and Reynolds numbers M and Re_D, inlet boundary-layer thickness δ, and intended Reynolds number Re_θ based on the nozzle-exit boundary-layer momentum thickness.

M	Re_D	δ_0/r_0	Re_θ
0.9	8.3×10^4	0.09	~ 480
0.9	5×10^4	0.15	~ 480
0.9	3×10^4	0.25	~ 480
0.9	1.8×10^4	0.42	~ 480

B. LES procedure and numerical methods

The LES are carried out using a solver of the three-dimensional filtered compressible Navier-Stokes equations in cylindrical coordinates (r, θ, z) based on low-dissipation and low-dispersion explicit schemes. The axis singularity is taken into account by the method of Mohseni & Colonius.[35] To alleviate the time-step restriction near the cylindrical origin, the derivatives in the azimuthal direction around the axis are calculated at coarser resolutions than permitted by the grid.[36] Fourth-order eleven-point centered finite differences are used for spatial discretization, and a second-order six-stage Runge-Kutta algorithm is implemented for time integration.[37] A sixth-order eleven-point centered filter[38] is applied explicitly to the flow variables every time step. Non-centered finite differences and filters are also used near the pipe walls and the grid boundaries.[31,39] The radiation conditions of Tam & Dong[40] are finally applied at all boundaries, with the addition at the outflow of a sponge zone combining grid stretching and Laplacian filtering.[41]

In the simulations, the explicit filtering is employed to remove grid-to-grid oscillations, but also as a subgrid high-order dissipation model to relax turbulent energy from scales at wave numbers close to the grid cut-off wave number while leaving larger scales mostly unaffected.[42–44] With this in mind, the reliability of the LES fields obtained for a jet at $\mathrm{Re}_D = 10^5$ with $u'_e/u_j = 9\%$ and $\delta_0 = 0.15r_0$ using the same grid as in this study has been assessed in Bogey *et al.*[32] based on the tranfer functions associated with molecular viscosity, relaxation filtering and time integration. Viscosity was shown to be the dominant dissipation mechanism for scales discretized at least by seven points per wavelength. The physics of the larger turbulent structures is therefore unlikely to be governed by numerical or subgrid-modeling dissipation, implying in particular that the effective flow Reynolds number should not be artificially decreased. These remarks certainly equally hold for the present simulations dealing with jets at lower Reynolds numbers.

C. Simulation parameters

As reported in table 3, the LES are performed using a grid containing $n_r \times n_\theta \times n_z = 256 \times 1024 \times 962 = 252$ million points. There are 169 points along the pipe nozzle, 77 points within the jet radius, and 31 points inside the inlet boundary layers. The physical domain, excluding the eighty-point outflow sponge zone, extends axially up to $L_z = 25r_0$, and radially up to $L_r = 9r_0$.

Table 3. Simulation parameters: numbers of grid points n_r, n_θ, n_z, mesh spacings Δr at $r = r_0$, $r_0\Delta\theta$, and Δz at $z = 0$, extents L_r, L_z of the physical domain, radial position r_c of the far-field extrapolation surface, and time duration T.

n_r, n_θ, n_z	$\Delta r/r_0$	$r_0\Delta\theta/r_0$	$\Delta z/r_0$	L_r, L_z	r_c/r_0	Tu_j/r_0
$256, 1024, 962$	0.36%	0.61%	0.72%	$9r_0, 25r_0$	6.5	375

The mesh spacing is uniform in the azimuthal direction, with $r_0\Delta\theta = 0.0061r_0$. In the axial direction, the mesh size is minimum between $z = -r_0$ and $z = 0$, with $\Delta z = 0.0072r_0$. It increases upstream of $z = -r_0$, but also downstream of the nozzle at stretching rates lower than 1% allowing to reach $\Delta z = 0.065r_0$ at $z = 13.3r_0$. In the radial direction, the mesh size is minimum around $r = r_0$, with $\Delta r = 0.0036r_0$. The maximum mesh size, obtained for $r \geq 3r_0$, is equal to $\Delta r = 0.081r_0$, yielding a Strouhal number of $\mathrm{St}_D = fD/u_j = 6.9$ for an acoustic wave discretized by four points par wavelength, where f is the time frequency.

The grid quality has been discussed in Bogey *et al.*[32] for a jet at $\mathrm{Re}_D = 10^5$ with $u'_e/u_j = 9\%$, $\delta_0 = 0.15r_0$ and $\mathrm{Re}_\theta = 900$. The ratios between the integral length scales of the axial fluctuating velocity and the mesh sizes along the lip line were shown to fall between 7 and 10. The properties of the nozzle-exit turbulence and of the shear-layer flow fields were moreover found to be practically grid-converged. Based on these results, there seems little doubt that the grid resolution is appropriate for the present jets with $\delta_0 = 0.15r_0$, $0.25r_0$ or $0.42r_0$. Indeed they display as thick or thicker mixing layers and lower diameter-based Reynolds numbers than the jet mentioned above, both of which points argue in favour of numerical accuracy. The resolution is also probably sufficient for the two jets with thinner initial shear layers with $\delta_0 = 0.09r_0$, because of the momentum Reynolds numbers $\mathrm{Re}_\theta \simeq 300$ and 480 which are much lower than that of $\mathrm{Re}_\theta \simeq 900$ in the reference jet. This should lead, for instance, to a reduction by at least 25% of the integral length scales according to a recent work.[24] Note that the solutions obtained for the four jets at $\mathrm{Re}_\theta \simeq 480$ will later confirm the grid quality in the present LES.

The simulation time, given in table 3, is equal to $375r_0/u_j$ in all cases. Density, velocity components and pressure are recorded from time $t = 100r_0/u_j$ at every point along the jet axis, and on the two surfaces at

$r = r_0$ and $r = r_c = 6.5r_0$, at a sampling frequency allowing the computation of spectra up to a Strouhal number of 20. The velocity spectra are evaluated from overlapping samples of duration $27.4r_0/u_j$. The flow statistics are determined from $t = 175r_0/u_j$, and they are averaged in the azimuthal direction.

The simulations have been performed using NEC SX-8 computers, on 7 processors using OpenMP, leading to a CPU speed of around 36 Gflops. Each LES required around 7,000 CPU hours and 60 Gb of memory for 164,000 time steps.

D. Far-field extrapolation

The LES near fields are propagated to the acoustic far field by solving the isentropic linearized Euler equations (ILEE) in cylindrical coordinates.[32,34,45] The extrapolation is performed from the LES velocity and pressure fluctuations at $r = r_c = 6.5r_0$. These data are interpolated onto a cylindrical surface discretized by an axial mesh spacing of $\Delta z = 0.065r_0$. They are then imposed at the bottom boundary of the grid on which the ILEE are solved using the same numerical methods as in the LES. This grid contains $845 \times 256 \times 1155$ points, and extends axially from $z = -16.6r_0$ to $58.2r_0$ and radially up to $r = 61.4r_0$. The grid spacings are uniform with $\Delta r = \Delta z = 0.065r_0$, yielding $\mathrm{St}_D = 8.6$ for an acoustic wave at four points per wavelength. After a propagation time of $t = 60r_0/u_j$, pressure is recorded around the jets at a distance of $60r_0$ from $z = r = 0$, where far-field acoustic conditions are expected to apply according to the experiments of Ahuja *et al.*,[46] during a period of $250r_0/u_j$. Pressure spectra are evaluated using overlapping samples of duration $38r_0/u_j$, and they are averaged in the azimuthal direction.

III. Results

In this section, the main aerodynamic and acoustic results obtained for the jets at $\mathrm{Re}_D = 5 \times 10^4$ are first presented. Those for the jets at $\mathrm{Re}_\theta \simeq 480$ are then shown and compared.

A. Jets at $\mathrm{Re}_D = 5 \times 10^4$

1. *Nozzle-exit conditions*

The profiles of mean and rms axial velocities obtained at the nozzle exit for the four jets at $\mathrm{Re}_D = 5 \times 10^4$ defined in table 1 are represented in figure 1. In figure 1(a), as intended, the mean velocity profiles look like the Blasius laminar profiles imposed at the pipe-nozzle inlet. They are characterized by shape factors between $H = 2.25$ and $H = 2.30$, and by momentum thicknesses $\delta_\theta(0) = 0.0119r_0$, $0.0191r_0$, $0.0308r_0$ and $0.0507r_0$, yielding Reynolds numbers $\mathrm{Re}_\theta = 304$, 486, 782 and 1288, as indicated in table 4. The effects of viscosity on the jet mixing layers can consequently be expected[24] to vary significantly with the ratio δ_0/r_0. In figure 1(b), the peak turbulence intensities u'_e/u_j are also observed to be close to 9% in all cases, see exact values in table 4. The initial flow conditions in the present jets therefore correspond to those found in highly disturbed, or nominally (not fully) turbulent boundary layers. Similar conditions were measured for instance by Batt,[47] Hussain & Zedan[16] and Zaman[6,7] in tripped jets with nozzle-exit parameters $u'_e/u_j \simeq 10\%$ and $\mathrm{Re}_\theta = 400$, $u'_e/u_j \simeq 6\%$ and $184 \leq \mathrm{Re}_\theta \leq 349$, and $u'_e/u_j \simeq 9\%$ and $900 \leq \mathrm{Re}_\theta \leq 2250$, respectively.

Table 4. Nozzle-exit conditions for the jets at $\mathrm{Re}_D = 5 \times 10^4$: peak turbulence intensity u'_e/u_j, shape factor H and momentum thickness $\delta_\theta(0)$ of the boundary layers, and Reynolds number Re_θ based on $\delta_\theta(0)$.

δ_0/r_0	u'_e/u_j	H	$\delta_\theta(0)/r_0$	Re_θ
0.09	9.14%	2.25	0.0119	304
0.15	9.20%	2.30	0.0191	486
0.25	9.15%	2.26	0.0308	782
0.42	9.12%	2.29	0.0507	1288

2. *Vorticity and pressure snapshots*

As first illustrations of the jet flow and noise characteristics, snapshots of the vorticity norm and fluctuating pressure given by the LES are provided. Vorticity fields obtained up to $z = 8r_0$ in the mixing layers are

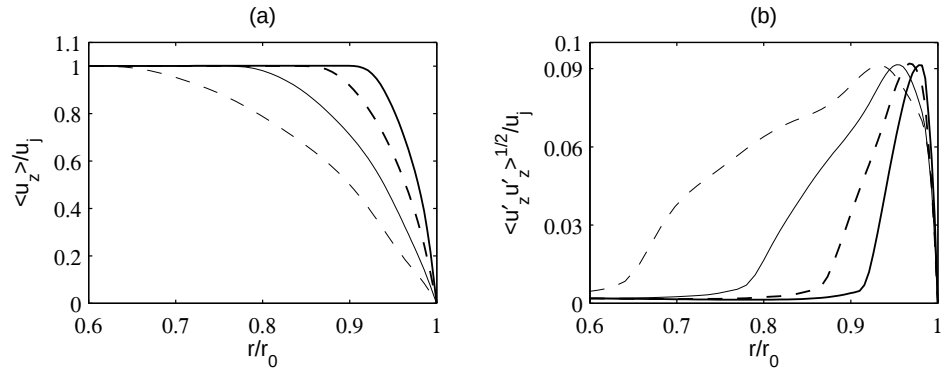

Figure 1. Profiles at $z = 0$ (a) of mean axial velocity $< u_z >$ and (b) of the rms values of fluctuating axial velocity u'_z for the jets at $\mathrm{Re}_D = 5 \times 10^4$ with an inlet boundary-layer thickness ——— $\delta_0 = 0.09r_0$, – – – $\delta_0 = 0.15r_0$, ——— $\delta_0 = 0.25r_0$, – – – $\delta_0 = 0.42r_0$.

first presented in figure 2. The difference in shear-layer thickness appears clearly in the vicinity of the nozzle exit, but is not obvious farther downstream, typically for $z \geq 4r_0$. This may suggest a slower development as the ratio δ_0/r_0 rises.

In order to perform relevant comparisons between the mixing-layer vorticity fields, a normalization based on the initial momentum thickness $\delta_\theta(0)$ is applied. The vorticity snapshots thus obtained up to $z = 225\delta_\theta(0)$, corresponding to $z = 2.7r_0$, $4.3r_0$, $6.9r_0$ and $11.4r_0$ with increasing δ_0, are shown in figure 3. For the jet with $\delta_0 = 0.09r_0$, large-scale structures resembling the coherent vortical structures revealed by the visualizations of Brown & Roshko[22] are well visible in figure 3(a). As the nozzle-exit boundary layers become thicker, such large-scale structures are however more difficult to observe, and small-scale turbulence gradually strengthens. The mixing-layer spreading rate seems also reduced, see for instance in figure 3(d) for the jet with $\delta_0 = 0.42r_0$. These trends are in agreement with those found in the recent work of Bogey *et al.*[24] on tripped jets with a fixed $\delta_0 = 0.15r_0$ at Reynolds numbers Re_D between 2.5×10^4 and 2×10^5, and Re_θ varying from 256 to 1856. They can therefore be attributed to viscosity effects as Re_θ increases with δ_0 in the present jets.

Snapshots of the vorticity norm up to $z = 20r_0$ in the jets, and of the near-field pressure fluctuations outside are displayed in figure 4. The jet overall developments are not seen to fundamentally differ. The sound field, on the contrary, changes appreciably with the initial shear-layer thickness in terms of both structure and level. Compare for example figure 4(a) and figure 4(d). In the jet with $\delta_0 = 0.09r_0$, strong acoustic waves are generated in the mixing layers around $z = 3r_0$. This is visibly not the case in the jet with $\delta_0 = 0.42r_0$, for which the emitted noise appears much weaker. These observations match those made in our previous LES focusing on the Reynolds number effects in jets.[24]

3. Shear-layer development

To quantify the influence of the ratio δ_0/r_0 on the shear layers of the present jets at $\mathrm{Re}_D = 5 \times 10^4$, the variations between $z = 0$ and $z = 10r_0$ of the momentum thickness δ_θ and of the maximum rms values of the axial velocity u'_z are presented in figure 5. As the nozzle-exit boundary-layer thickness increases, the mixing layers are found to develop more slowly in figure 5(a), resulting in curves of δ_θ crossing one another, hence in smaller shear-layer thickness for larger δ_0 farther downstream. At the same time, reduced turbulence levels are obtained in figure 5(b). The rms axial velocity profiles thus reach peak values of $0.171u_j$ for $\delta_0 = 0.09r_0$, $0.164u_j$ for $\delta_0 = 0.15r_0$, $0.154u_j$ for $\delta_0 = 0.25r_0$, and only $0.148u_j$ for $\delta_0 = 0.42r_0$, refer to table 5 for other velocity components. They also show an overshoot around $z = 1.5r_0$ and $z = 3.5r_0$ for $\delta_0 = 0.09r_0$ and $\delta_0 = 0.15r_0$, respectively, whereas they grow nearly monotonically in the two other cases. The shear-layer transition is therefore smoother in the jets with thicker exit boundary layers.

Using a scaling with the initial shear-layer momentum thickness $\delta_\theta(0)$, the variations of $\delta_\theta/\delta_\theta(0)$ and of the maximum rms values of u'_z are plotted in figures 6(a) and 6(b) as a function of $z/\delta_\theta(0)$ from $z = 0$ up to $z = 250\delta_\theta(0)$. The profiles clearly indicate that the mixing-layer spreading rates and the turbulence intensities both decrease with increasing δ_0. They are very similar to those obtained in a recent computational study[24] for axisymmetric shear layers with initial parameters $u'_e/u_j \simeq 9\%$ and Re_θ rising from 256 to 1856.

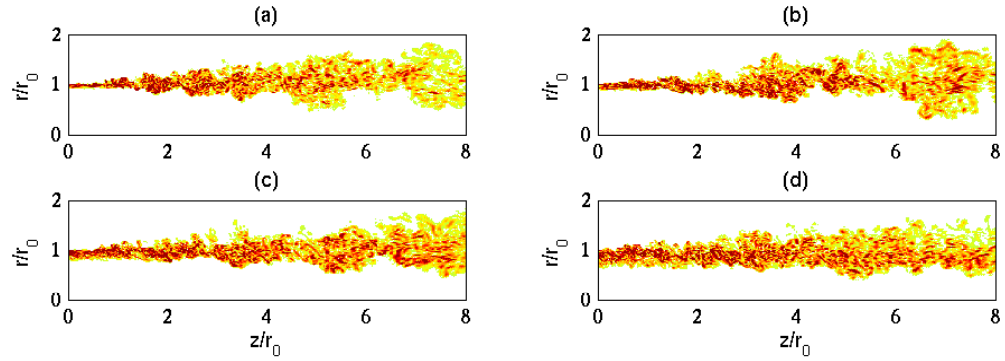

Figure 2. Snapshots in the (z, r) plane of vorticity norm $|\omega|$ downstream of the nozzle up to $z = 8r_0$ for the jets at $\mathrm{Re}_D = 5 \times 10^4$ with (a) $\delta_0 = 0.09r_0$, (b) $\delta_0 = 0.15r_0$, (c) $\delta_0 = 0.25r_0$, (d) $\delta_0 = 0.42r_0$. The color scale ranges up to the level of $17.5u_j/r_0$, $15.5u_j/r_0$, $13.5u_j/r_0$ and $11.5u_j/r_0$, respectively. Only $r \geq 0$ is shown.

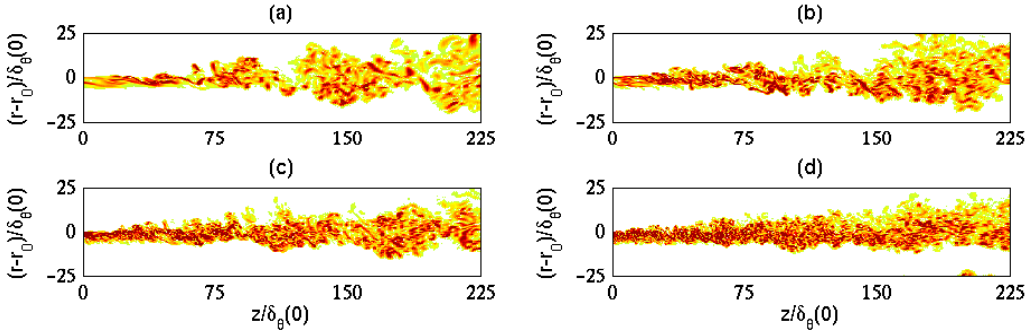

Figure 3. Snapshots in the (z, r) plane of vorticity norm $|\omega|$, represented using axes normalized by $\delta_\theta(0)$, for the jets at $\mathrm{Re}_D = 5 \times 10^4$ (a) $\delta_0 = 0.09r_0$, (b) $\delta_0 = 0.15r_0$, (c) $\delta_0 = 0.25r_0$, (d) $\delta_0 = 0.42r_0$. The color scale ranges up to the level of $0.42u_j/\delta_\theta(0)$.

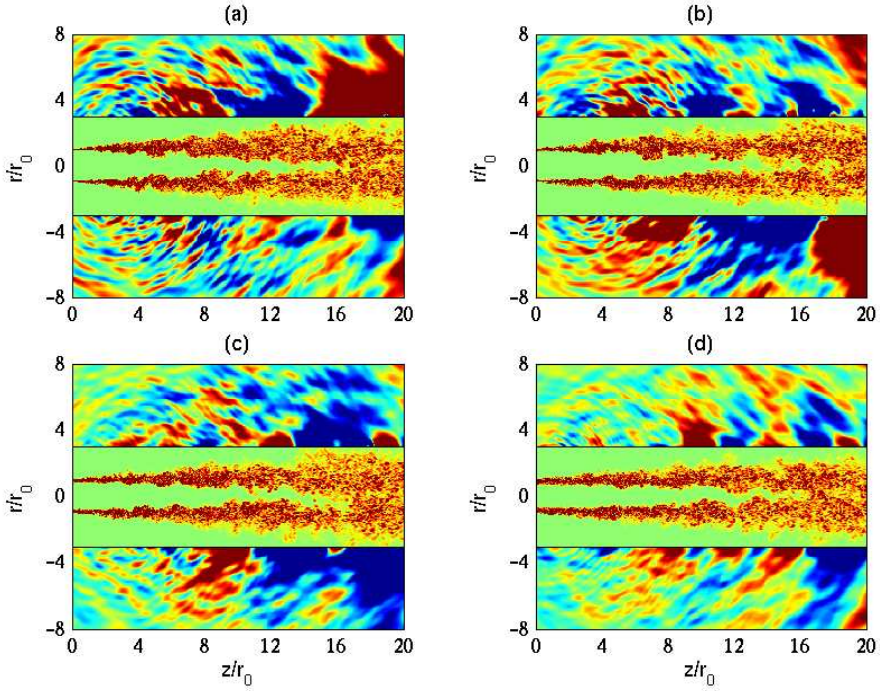

Figure 4. Snapshots in the (z, r) plane of vorticity norm $|\omega|$ in the flow and of fluctuating pressure $p - p_{amb}$ outside, for the jets at $\mathrm{Re}_D = 5 \times 10^4$ with (a) $\delta_0 = 0.09r_0$, (b) $\delta_0 = 0.15r_0$, (c) $\delta_0 = 0.25r_0$, (d) $\delta_0 = 0.42r_0$. The color scales range up to the level of $5.5u_j/r_0$ for the vorticity, and from -70 to 70 Pa for the pressure.

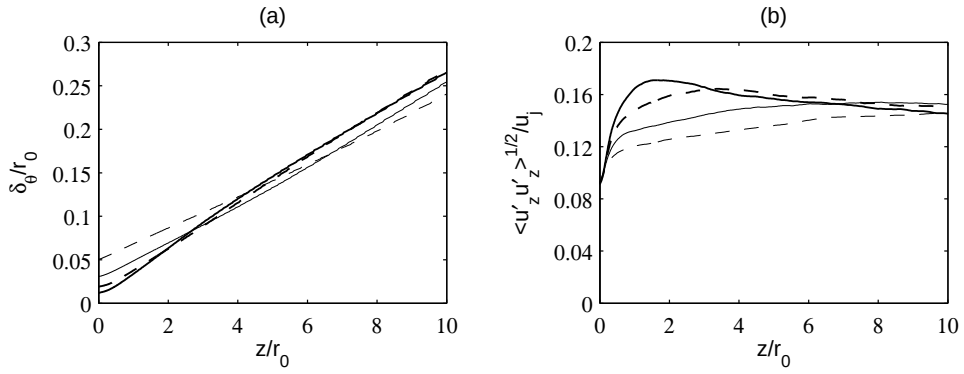

Figure 5. Variations with z/r_0 (a) of shear-layer momentum thickness δ_θ and (b) of peak rms values of fluctuating axial velocity u'_z for the jets at $Re_D = 5 \times 10^4$ with ——— $\delta_0 = 0.09r_0$, – – – $\delta_0 = 0.15r_0$, ——— $\delta_0 = 0.25r_0$, – – – $\delta_0 = 0.42r_0$.

Table 5. Peak values of turbulence intensities in the jets at $Re_D = 5 \times 10^4$.

δ_0/r_0	$<u'^2_z>^{1/2}/u_j$	$<u'^2_r>^{1/2}/u_j$	$<u'^2_\theta>^{1/2}/u_j$	$<u'_r u'_z>/u_j$
0.09	17.1%	13.3%	15.0%	11.0%
0.15	16.4%	12.3%	13.9%	10.1%
0.25	15.4%	11.3%	13.0%	9.3%
0.42	14.8%	10.7%	12.3%	8.8%

With Reynolds numbers Re_θ ranging from 304 for $\delta_0 = 0.09r_0$ up to 1288 for $\delta_0 = 0.42r_0$, the present results are therefore most probably due to Reynolds number effects, as mentioned previously.

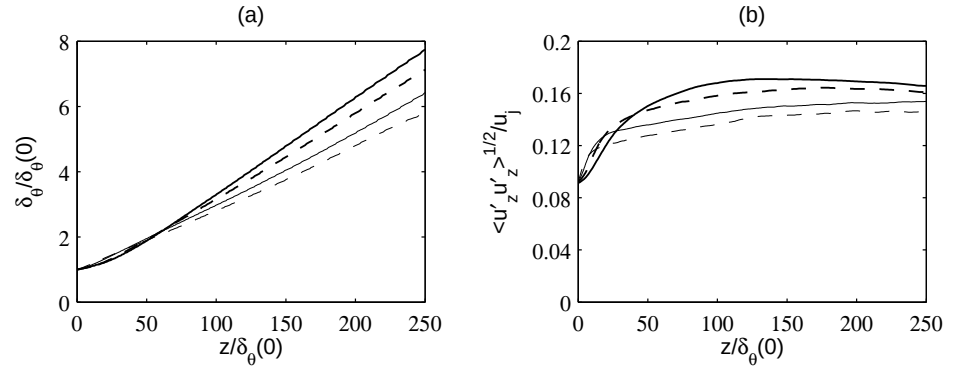

Figure 6. Variations with $z/\delta_\theta(0)$ (a) of shear-layer momentum thickness $\delta_\theta/\delta_\theta(0)$ and (b) of peak rms values of velocity u'_z for the jets at $Re_D = 5 \times 10^4$ with ——— $\delta_0 = 0.09r_0$, – – – $\delta_0 = 0.15r_0$, ——— $\delta_0 = 0.25r_0$, – – – $\delta_0 = 0.42r_0$.

4. Jet development

The variations of the mean and rms axial velocities on the jet axis are presented in figure 7. Measurements[4,48,49] available for Mach number 0.9 jets at high Reynolds numbers $Re_D \geq 5 \times 10^5$, which can be expected to be initially turbulent, are also depicted for the comparison. Increasing the initial shear-layer thickness appears in figure 7(a) to reduce the potential core length from $z_c = 15.8r_0$ for $\delta_0 = 0.09r_0$ down to $z_c = 13.7r_0$ for $\delta_0 = 0.42r_0$, where z_c is arbitrarily defined by $<u_z>(z = z_c) = 0.95u_j$, as reported in table 6. It may also result in a more rapid velocity decay downstream of the potential core. Regarding the centerline axial turbulence intensities in figure 7(b), they are rather similar with peak values around $0.115u_j$, except for the jet with $\delta_0 = 0.25r_0$ in which the peak value is higher and equal to $0.136u_j$, refer to table 6 for the radial velocity component showing a similar trend. The centerline velocity profiles moreover correspond fairly well

to the measurements, which are certainly obtained for jets with various exit boundary-layer conditions.

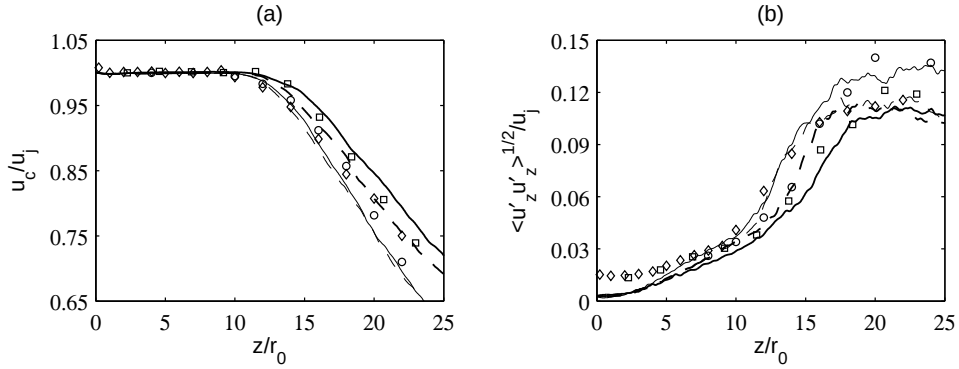

Figure 7. Variations (a) of centerline mean axial velocity u_c and (b) of centerline rms values of velocity u'_z for the jets at $Re_D = 5 \times 10^4$ with ——— $\delta_0 = 0.09r_0$, – – – $\delta_0 = 0.15r_0$, ——— $\delta_0 = 0.25r_0$, – – – $\delta_0 = 0.42r_0$. Measurements for jets at M = 0.9 and $Re_D \geq 5 \times 10^5$: ∘ Lau *et al.*,[48] □ Arakeri *et al.*,[4] ◇ Fleury *et al.*[49]

Table 6. Axial position of the end of the potential core z_c, and peak rms values of fluctuating velocities u'_z and u'_r on the axis for the jets at $Re_D = 5 \times 10^4$.

δ_0/r_0	z_c/r_0	$<u'^2_z>^{1/2}/u_j$	$<u'^2_r>^{1/2}/u_j$
0.09	15.8	11.1%	9.2%
0.15	14.7	11.4%	9.4%
0.25	14.1	13.6%	10.4%
0.42	13.7	11.7%	9.7%

5. Acoustic fields

The main properties of the acoustic fields computed at 60 radii from the nozzle exit using the wave extrapolation method described in section II.D are investigated. The sound pressure levels obtained in this way are first displayed in figure 8. The jets with thicker initial shear layers are found to generate lower noise. The decrease of the sound levels is particularly significant for the jet with $\delta_0 = 0.42r_0$, with a difference of about 2.5 and 3 dB with respect to the jets with $\delta_0 = 0.09r_0$ and $0.15r_0$ at the radiation angles $\phi = 40^o$ and $\phi = 90^o$, respectively, see in table 7. This leads for this jet to a good agreement with measurements[50–52] available for Mach number 0.9 jets at high Reynolds numbers $Re_D \geq 5 \times 10^5$. The present noise reduction is very probably due to the weakening of the large-scales structures, and of their interactions, and to the lowering of the turbulence intensities in the mixing layers. It most likely results from Reynolds number effects[24] since the value of Re_θ increases with δ_0. It is interesting to point out here that increasing the initial shear-layer thickness in jets at a fixed Re_D appears to cause contrary results on the sound field depending on the laminar or turbulent flow state at the nozzle exit. With rising δ_0, more precisely, the noise levels become stronger for fully laminar initial conditions,[31] whereas they get weaker for highly disturbed initial conditions as in this study.

Table 7. Overall sound pressure levels at $60r_0$ from the nozzle exit at $\phi = 40^o$ and $\phi = 90^o$ for the jets at $Re_D = 5 \times 10^4$.

δ_0/r_0	$\phi = 40^o$	$\phi = 90^o$
0.09	116.3 dB	109.2 dB
0.15	116.6 dB	109.2 dB
0.25	116.0 dB	108.1 dB
0.42	114.0 dB	106.3 dB

The pressure spectra calculated for the jets at $60r_0$ from the nozzle exit at the angles $\phi = 40^o$ and 90^o are

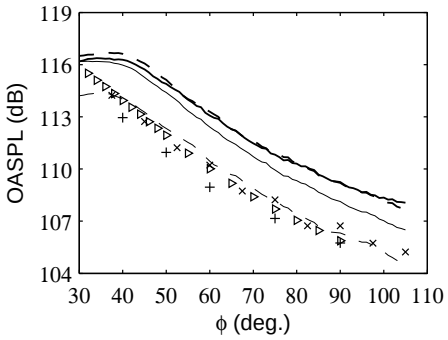

Figure 8. Overall sound pressure levels (OASPL) at $60r_0$ from the nozzle exit, as a function of the angle ϕ relative to the jet direction, for the jets at $\mathrm{Re}_D = 5 \times 10^4$ with ——— $\delta_0 = 0.09r_0$, – – – $\delta_0 = 0.15r_0$, ——— $\delta_0 = 0.25r_0$, – – – $\delta_0 = 0.42r_0$. Measurements for jets at $\mathrm{Re}_D \geq 5 \times 10^5$: + Mollo-Christensen *et al.*,[50] × Lush,[51] ▷ Bogey *et al.*[52]

finally given in figure 9 as a function of Strouhal number St_D, and compared with experimental data for jets at high Reynolds numbers.[52,53] As the initial shear-layer thickness of the jets increases, high-frequency noise components are significantly reduced. This is particularly true at $\phi = 90^\circ$ in figure 9(b), where about 10 dB is for instance observed at $\mathrm{St}_D = 3.2$ between the sound levels of the jets with $\delta_0 = 0.09r_0$ and $\delta_0 = 0.42r_0$. At this radiation angle, with rising δ_0, the acoustic levels also decrease at lower frequencies down to $\mathrm{St}_D \simeq 0.3$. Similar results can be seen for the angle $\phi = 40^\circ$ in figure 9(a). In this case, the jet with $\delta_0 = 0.42r_0$ clearly generate weaker noise with respect to the other jets down to Strouhal number $\mathrm{St}_D = 0.1$.

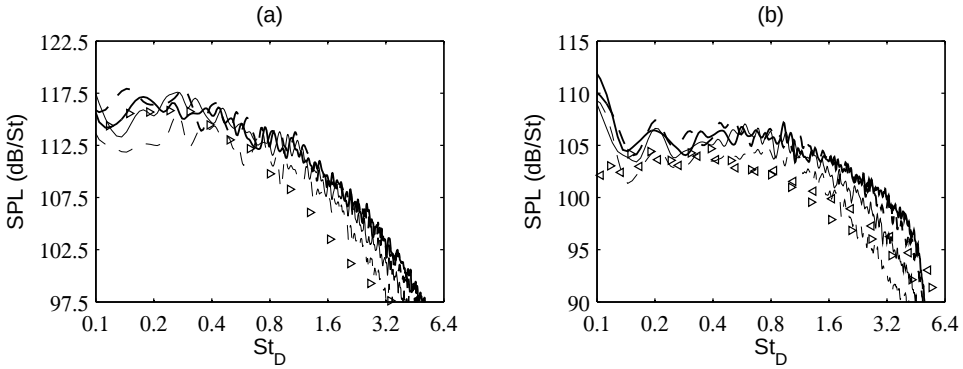

Figure 9. Sound pressure levels (SPL) at $60r_0$ from the nozzle exit, as a function of St_D, at the angles ϕ of (a) 40° and (b) 90° for the jets at $\mathrm{Re}_D = 5 \times 10^4$ with ——— $\delta_0 = 0.09r_0$, – – – $\delta_0 = 0.15r_0$, ——— $\delta_0 = 0.25r_0$, – – – $\delta_0 = 0.42r_0$. Measurements for jets at $\mathrm{Re}_D \geq 7.8 \times 10^5$: ◁ Tanna,[53] ▷ Bogey *et al.*[52]

B. Jets at $\mathrm{Re}_\theta \simeq 480$

1. Nozzle-exit conditions

The profiles of mean and rms axial velocities obtained at $z = 0$ for the jets at $\mathrm{Re}_\theta \simeq 480$ defined in table 2 are presented in figures 10(a) and 10(b). They are nearly identical to those shown in figures 1(a) and 1(b), indicating that the nozzle-exit conditions in the jets at $\mathrm{Re}_D = 5 \times 10^4$ and at $\mathrm{Re}_\theta \simeq 480$ can be considered as effectively the same except for the Reynolds numbers. As reported in table 8, the exit boundary layers are characterized by shape factors $2.22 \leq H \leq 2.32$, peak turbulence intensities $9.12\% \leq u'_e/u_j \leq 9.20\%$, and momentum thicknesses $\delta_\theta(0) = 0.0115r_0$, $0.0191r_0$, $0.0313r_0$ or $0.0515r_0$. The momentum Reynolds numbers in the four jets are consequently very similar, as desired, and lie within the range $471 \leq \mathrm{Re}_\theta \leq 487$. In this way, the differences in mixing-layer properties which will be observed in what follows could not be attributed to Reynolds number effects, but only to the variations of the ratio δ_0/r_0.

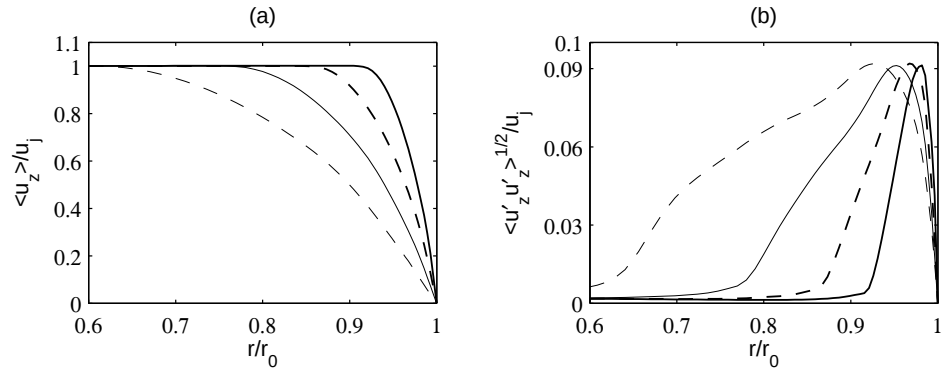

Figure 10. Profiles at $z = 0$ (a) of mean axial velocity $< u_z >$ and (b) of the rms values of fluctuating axial velocity u'_z for the jets at $\mathrm{Re}_\theta \simeq 480$ with an inlet boundary-layer thickness ——— $\delta_0 = 0.09r_0$, − − − $\delta_0 = 0.15r_0$, ——— $\delta_0 = 0.25r_0$, − − − $\delta_0 = 0.42r_0$.

Table 8. Nozzle-exit conditions for the jets at $\mathrm{Re}_\theta \simeq 480$: peak turbulence intensity u'_e/u_j, shape factor H and momentum thickness $\delta_\theta(0)$ of the boundary layers, and Reynolds number Re_θ based on $\delta_\theta(0)$.

δ_0/r_0	u'_e/u_j	H	$\delta_\theta(0)/r_0$	Re_θ
0.09	9.13%	2.32	0.0115	487
0.15	9.20%	2.30	0.0191	486
0.25	9.12%	2.22	0.0313	477
0.42	9.19%	2.25	0.0515	471

2. Vorticity and pressure snapshots

Snapshots of the vorticity norm obtained up to $z = 8r_0$ in the shear layers are displayed in figure 11. Compare, for instance, figure 11(a) for $\delta_0 = 0.09r_0$ and figure 11(d) for $\delta_0 = 0.42r_0$. It seems, contrary to what was noted for the jets at $\mathrm{Re}_D = 5 \times 10^4$ in figure 2, that mixing layers with smaller thickness at the nozzle exit remain thinner than the others farther dowsntream, which will be checked later.

As previously, the vorticity fields in the shear layers are also represented using x and y-axes normalized by the initial momentum thickness $\delta_\theta(0)$. The four snapshots thus obtained up to $z = 225\delta_\theta(0)$ are shown in figure 12. They are very much alike regardless of δ_0/r_0, which is expected given that the Reynolds numbers Re_θ are nearly identical. There is no notable change in the mixing-layer spreading rate, nor in the distribution between large and small turbulent scales, unlike the findings observed in figure 3 for the jets at $\mathrm{Re}_D = 5 \times 10^4$. Large-scale coherent-like vortical structures are in particular observed in all cases.

Snapshots of the vorticity norm up to $z = 20r_0$ in the jets, and of the pressure fluctuations outside, are finally provided in figure 13. With increasing the nozzle-exit boundary-layer thickness, the jet flows appear to develop more rapidly, leading to shorter potential cores, visibly ending around $z = 16r_0$ in figure 13(a) for $\delta_0 = 0.09r_0$, but only around $z = 10r_0$ in figure 13(d) for $\delta_0 = 0.42r_0$. The sound pressure fields are also modified. For all jets, strong acoustic waves are emitted in the mixing layers. They are of roughly similar amplitude, but they have distinctly larger wavelengths as the value of δ_0/r_0 rises.

3. Shear-layer development

The variations between $z = 0$ and $z = 10r_0$ of the shear-layer momentum thickness δ_θ and of the maximum rms values of the axial velocity u'_z are presented in figure 14. The profiles of δ_θ are seen not to intersect in figure 14(a), implying that the larger the nozzle-exit boundary-layer thickness, the thicker the mixing layers farther downstream whatever the axial position. The profiles of turbulence intensities also do not appear to differ much in figure 14(b). The levels of axial velocity fluctuations naturally increase more rapidly with larger δ_0/r_0, but they reach peak values, typically at $z \simeq 1.5r_0$ for $\delta_0 = 0.09r_0$, $z \simeq 3r_0$ for $\delta_0 = 0.15r_0$, $z \simeq 4.5r_0$ for $\delta_0 = 0.25r_0$, and $z \simeq 1.5r_0$ for $\delta_0 = 0.42r_0$, which are very close. Peak values between $0.160u_j$ and $0.164u_j$ are indeed found, see also in table 9 for the rms values of radial and azimuthal velocities u'_r and u'_θ and the Reynolds shear stress $< u'_r u'_z >$. It can further be emphasized that for all jets

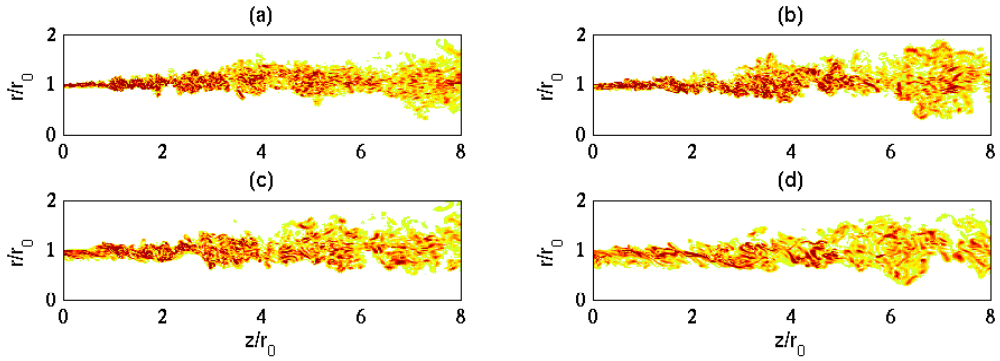

Figure 11. Snapshots in the (z, r) plane of vorticity norm $|\omega|$ downstream of the nozzle up to $z = 8r_0$ for the jets at $\mathrm{Re}_\theta \simeq 480$ with (a) $\delta_0 = 0.09r_0$, (b) $\delta_0 = 0.15r_0$, (c) $\delta_0 = 0.25r_0$, (d) $\delta_0 = 0.42r_0$. The color scale ranges up to the level of $17.5u_j/r_0$, $15.5u_j/r_0$, $13.5u_j/r_0$ and $11.5u_j/r_0$, respectively. Only $r \geq 0$ is shown.

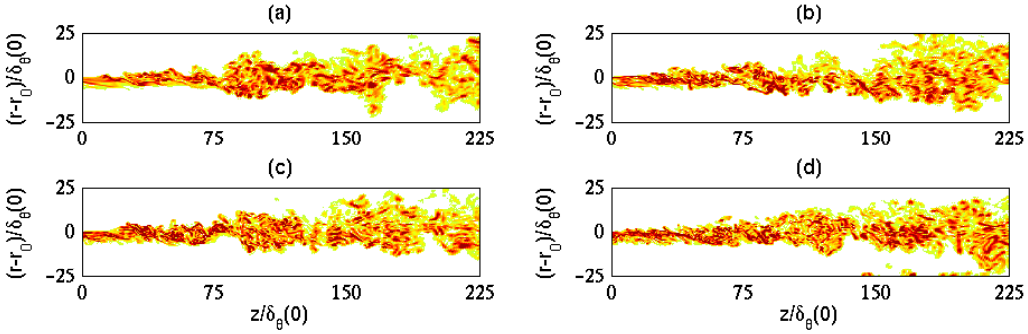

Figure 12. Snapshots in the (z, r) plane of vorticity norm $|\omega|$, represented using axes normalized by $\delta_\theta(0)$, for the jets at $\mathrm{Re}_\theta \simeq 480$ with (a) $\delta_0 = 0.09r_0$, (b) $\delta_0 = 0.15r_0$, (c) $\delta_0 = 0.25r_0$, (d) $\delta_0 = 0.42r_0$. The color scale ranges up to the level of $0.42u_j/\delta_\theta(0)$.

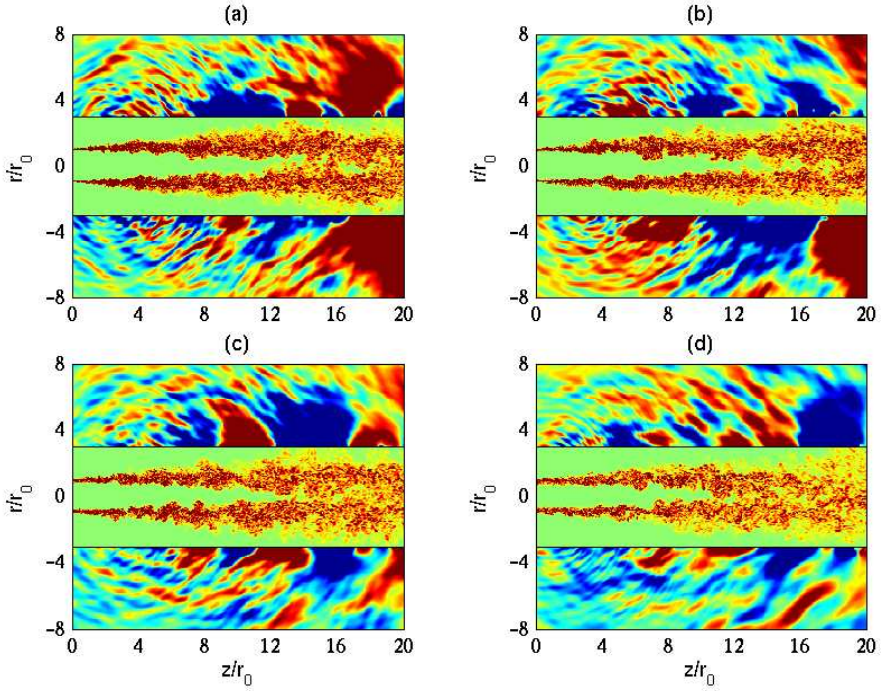

Figure 13. Snapshots in the (z, r) plane of vorticity norm $|\omega|$ in the flow and of fluctuating pressure $p - p_{amb}$ outside, for the jets at $\mathrm{Re}_\theta \simeq 480$ with (a) $\delta_0 = 0.09r_0$, (b) $\delta_0 = 0.15r_0$, (c) $\delta_0 = 0.25r_0$, (d) $\delta_0 = 0.42r_0$. The color scales range up to the level of $5.5u_j/r_0$ for the vorticity, and from -70 to 70 Pa for the pressure.

the turbulence intensity profiles display a hump, although modest, in the developing mixing layers.

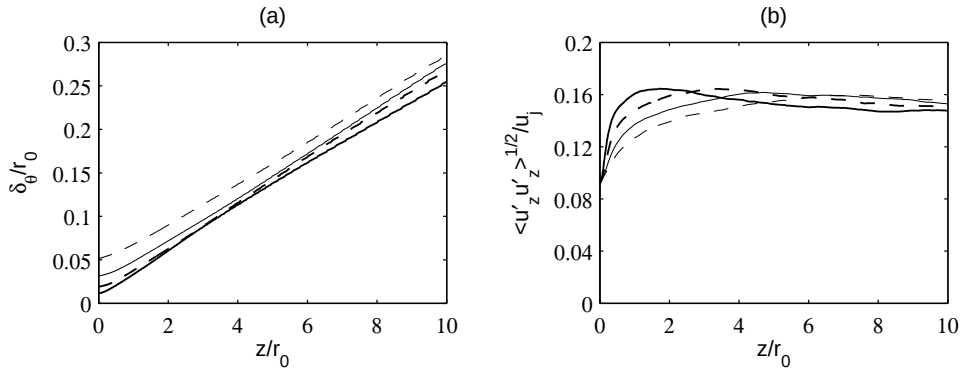

Figure 14. Variations with z/r_0 (a) of shear-layer momentum thickness δ_θ and (b) of peak rms values of fluctuating axial velocity u'_z for the jets at $Re_\theta \simeq 480$ with ——— $\delta_0 = 0.09r_0$, – – – $\delta_0 = 0.15r_0$, ——— $\delta_0 = 0.25r_0$, – – – $\delta_0 = 0.42r_0$.

Table 9. Peak values of turbulence intensities in the jets at $Re_\theta \simeq 480$.

δ_0/r_0	$<u'^2_z>^{1/2}/u_j$	$<u'^2_r>^{1/2}/u_j$	$<u'^2_\theta>^{1/2}/u_j$	$<u'_r u'_z>/u_j$
0.09	16.4%	12.7%	14.4%	10.4%
0.15	16.4%	12.3%	13.9%	10.1%
0.25	16.2%	12.0%	13.8%	9.9%
0.42	16.0%	11.6%	13.3%	9.6%

The variations of $\delta_\theta/\delta_\theta(0)$ and of the maximum rms values of u'_z are re-plotted in figures 15(a) and 15(b) as a function of $z/\delta_\theta(0)$ up to $z = 250\delta_\theta(0)$. The profiles obtained for the four jets with varying initial shear-layer thickness nearly superimpose, demonstrating that the flow transition in the present mixing layers at approximately the same Re_θ does not depend on the ratio δ_0/r_0, contrary to what happened in figure 6 for the jets at a fixed Re_D. This expected result moreover suggests grid-convergence of the LES solutions, confirming *a posteriori* the grid quality, discussed based on *a priori* arguments in section II.C, for all δ_0 in this study.

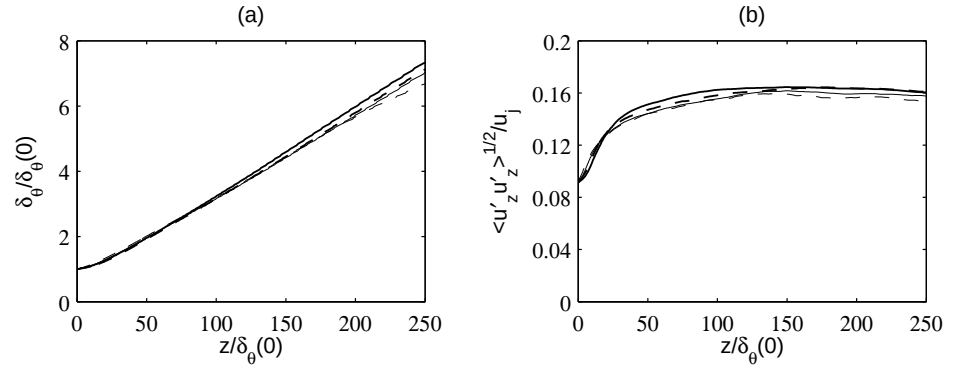

Figure 15. Variations with $z/\delta_\theta(0)$ (a) of shear-layer momentum thickness $\delta_\theta/\delta_\theta(0)$ and (b) of peak rms values of velocity u'_z for the jets at $Re_\theta \simeq 480$ with ——— $\delta_0 = 0.09r_0$, – – – $\delta_0 = 0.15r_0$, ——— $\delta_0 = 0.25r_0$, – – – $\delta_0 = 0.42r_0$.

4. Jet development

The centerline variations of the mean and rms axial velocities are presented in figure 16, together with corresponding measurements[4,48,49] for Mach number 0.9 jets at high Reynolds numbers $Re_D \geq 5 \times 10^5$. Larger initial shear-layer thickness clearly leads to shorter potential core lengths in figure 16(a), decreasing

from $z_c = 16r_0$ for $\delta_0 = 0.09r_0$ down to $z_c = 11.7r_0$ for $\delta_0 = 0.42r_0$ in table 6. Downstream of the potential core, the mean axial velocity then seems to decay at a higher rate. Significant discrepancies are also observed between the profiles of axial turbulence intensity in figure 16(b). In particular, they reach peaks of growing amplitude as δ_0 increases, namely of 11.1% for $\delta_0 = 0.09r_0$, 11.4% for $\delta_0 = 0.15r_0$, 12.5% for $\delta_0 = 0.25r_0$, and 13.6% for $\delta_0 = 0.42r_0$. A similar tendency is reported for the peak rms values of u'_r in table 10. The jet flow therefore appears to develop more rapidly with stronger velocity fluctuations with thicker nozzle-exit boundary layers.

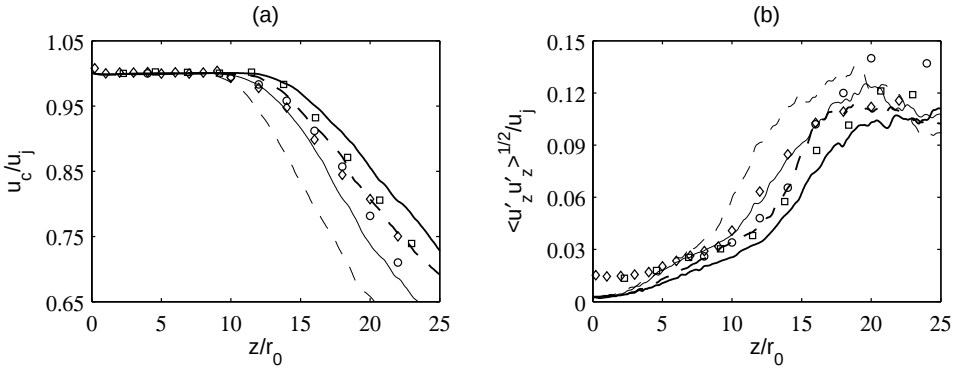

Figure 16. Variations (a) of centerline mean axial velocity u_c and (b) of centerline rms values of velocity u'_z for the jets at $\mathrm{Re}_\theta \simeq 480$ with ——— $\delta_0 = 0.09r_0$, – – – $\delta_0 = 0.15r_0$, ——— $\delta_0 = 0.25r_0$, – – – $\delta_0 = 0.42r_0$. Measurements for jets at M = 0.9 and $\mathrm{Re}_D \geq 5 \times 10^5$: ○ Lau *et al.*,[48] □ Arakeri *et al.*,[4] ◇ Fleury *et al.*[49]

Table 10. Axial position of the end of the potential core z_c, and peak rms values of fluctuating velocities u'_z and u'_r on the axis for the jets at $\mathrm{Re}_\theta \simeq 480$.

δ_0/r_0	z_c/r_0	$<u'^2_z>^{1/2}/u_j$	$<u'^2_r>^{1/2}/u_j$
0.09	16.0	11.1%	8.7%
0.15	14.7	11.4%	9.4%
0.25	13.7	12.5%	9.7%
0.42	11.7	13.6%	10.4%

5. Acoustic fields

The sound pressure levels calculated at $60r_0$ from the nozzle exit for the jets at $\mathrm{Re}_\theta \simeq 480$ are depicted in figure 17. For radiation angles relative to the flow direction higher than $\phi = 50^\circ$, the acoustic levels do not appear to differ much depending on the initial shear-layer thickness. In addition, no clear trend is observed. At $\phi = 90^\circ$, for instance, they vary from 108.2 dB for $\delta_0 = 0.42r_0$ up to 109.2 dB for $\delta_0 = 0.15r_0$, as evidenced in table 11. For smaller angles, however, they are found to unambiguously increase with the ratio δ_0/r_0, thus yielding, at $\phi = 40^\circ$, 115.6 dB for $\delta_0 = 0.09r_0$ but 117.2 dB for $\delta_0 = 0.42r_0$, see also in table 11. This result can be related to the strengthening of centerline velocity fluctuations previously noticed for larger δ_0/r_0. Moreover, with respect to experimental data[50–52] for jets at Mach number 0.9 and at diameter-based Reynolds numbers $\mathrm{Re}_D \geq 5 \times 10^5$, the sound levels are higher by about 3 dB, which is probably[24] due to the presence and interactions of large-scale structures in the mixing layers of the present jets at low Reynolds numbers Re_θ.

The pressure spectra evaluated at $60r_0$ from the nozzle exit at the angles $\phi = 40^\circ$ and 90° are finally shown as a function of Strouhal number St_D, and compared to measurements for high-Reynolds-number jets[52,53] in figure 18. As for the jets at $\mathrm{Re}_D = 5\times10^4$ in figure 9, the magnitude of high-frequency components at $\mathrm{St}_D \geq 2$ decreases as the nozzle-exit boundary-layer thickness increases. In this case, however, low-frequency noise does not appear to be reduced. Acoustic components below $\mathrm{St}_D = 0.8$, on the contrary, become stronger. The change is relatively moderate at $\phi = 90^\circ$ in figure 18(b), but is more marked at $\phi = 40^\circ$ in figure 18(a). One reason for that may be the higher turbulence intensities obtained at the end of the potential core with rising δ_0/r_0, leading probably to a stronger noise radiation in the downstream direction.[31,34,54–57]

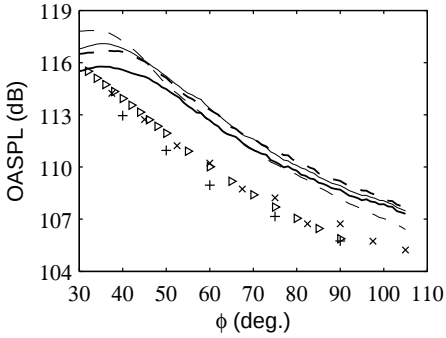

Figure 17. Overall sound pressure levels (OASPL) at $60r_0$ from the nozzle exit, as a function of the angle ϕ, for the jets at $\mathrm{Re}_\theta \simeq 480$ with ——— $\delta_0 = 0.09r_0$, – – – $\delta_0 = 0.15r_0$, ——— $\delta_0 = 0.25r_0$, – – – $\delta_0 = 0.42r_0$. Measurements for jets at $\mathrm{Re}_D \geq 5 \times 10^5$: + Mollo-Christensen *et al.*,[50] × Lush,[51] ▷ Bogey *et al.*[52]

Table 11. Overall sound pressure levels at $60r_0$ from the nozzle exit at $\phi = 40^\mathrm{o}$ and $\phi = 90^\mathrm{o}$ for the jets at $\mathrm{Re}_\theta \simeq 480$.

δ_0/r_0	$\phi = 40^\mathrm{o}$	$\phi = 90^\mathrm{o}$
0.09	115.6 dB	108.7 dB
0.15	116.6 dB	109.2 dB
0.25	116.8 dB	108.9 dB
0.42	117.2 dB	108.2 dB

Another reason may be the modification of the frequencies of the waves generated in the mixing layers, which is clearly visible in the pressure fields of figure 13. Based on previous work,[24] these components can furthermore be expected to be roughly centered around half the Strouhal number $\mathrm{St}_\theta = f\delta_\theta(0)/u_j \simeq 0.013$, giving $\mathrm{St}_D = 1.13$, 0.68, 0.42 and 0.25 for the jets with $\delta_0 = 0.09r_0$, $0.15r_0$, $0.25r_0$ and $0.42r_0$, respectively.

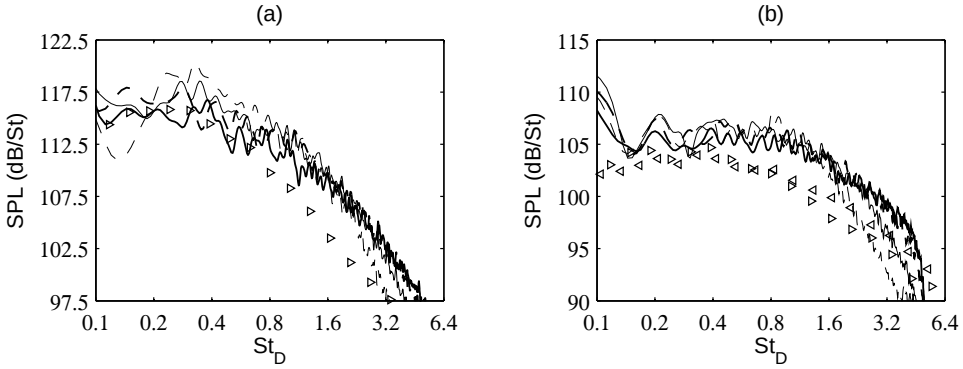

Figure 18. Sound pressure levels (SPL) at $60r_0$ from the nozzle exit, as a function of St_D, at the angles ϕ of (a) 40^o and (b) 90^o for the jets at $\mathrm{Re}_\theta \simeq 480$ with ——— $\delta_0 = 0.09r_0$, – – – $\delta_0 = 0.15r_0$, ——— $\delta_0 = 0.25r_0$, – – – $\delta_0 = 0.42r_0$. Measurements for jets at $\mathrm{Re}_D \geq 7.8 \times 10^5$: ◁ Tanna,[53] ▷ Bogey *et al.*[52]

IV. Summary and conclusion

In this paper, the influence of the nozzle-exit boundary-layer thickness on initially highly disturbed subsonic jets has been investigated for inlet boundary-layer thicknesses $0.09r_0 \leq \delta_0 \leq 0.42r_0$, diameter Reynolds numbers $1.8 \times 10^4 \leq \mathrm{Re}_D \leq 8.3 \times 10^4$ and momentum-thickness Reynolds numbers $304 \leq \mathrm{Re}_\theta \leq 1288$. Jets at a constant $\mathrm{Re}_D = 5 \times 10^4$ as well as jets at nearly identical $\mathrm{Re}_\theta \simeq 480$ have been considered, in order to distinguish between the effects of δ_0/r_0 and Re_θ. In that sense, this work is a direct continuation of and a complement to a recent study[24] dealing with the sensitivity to Reynolds number of tripped jets with a fixed $\delta_0 = 0.15r_0$ but at Reynolds numbers $2.5 \times 10^4 \leq \mathrm{Re}_D \leq 2 \times 10^5$, and consequently $256 \leq \mathrm{Re}_\theta \leq 1856$.

The main findings are summarized below, and illustrated in figures 19 and 20 using solid lines for the jets at $\mathrm{Re}_D = 5 \times 10^4$ and dashed lines for the jets at $\mathrm{Re}_\theta \simeq 480$. In figure 19(a), increasing the initial shear-layer thickness appears to shorten the jet potential core, but in jets at a constant diameter Reynolds number Re_D, this tendency may be countered by the effects of the Reynolds number Re_θ. Concerning the turbulence intensities, in figure 19(b), their peak values in the mixing layers (black lines) are seen to depend essentially on and to decrease with Re_θ, whereas those found on the jet axis (grey lines) increase appreciably with the ratio δ_0/r_0 for $\delta_0/r_0 \geq 0.15$. As a result, the far-field pressure levels are likely to significantly vary, as shown in figure 20(a) and 20(b) for the angles $\phi = 40^\mathrm{o}$ and 90^o. Thickening the nozzle-exit boundary layers for a fixed jet diameter, as in most experiments, generally leads to weaker sound levels at all radiation angles because of the corresponding increase of the Reynolds number Re_θ. In the case that the latter parameter does not vary much, however, rising δ_0/r_0 has a little impact on noise levels, except for a moderate strengthening in the downstream direction.

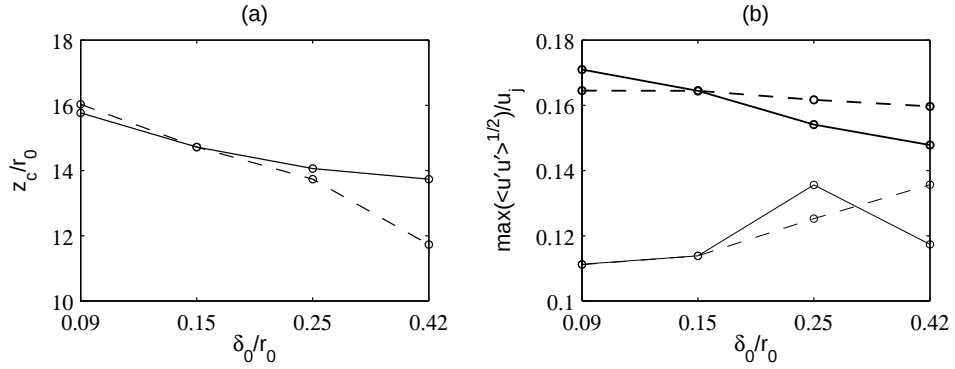

Figure 19. Variations with δ_0/r_0 (a) of the axial position of the end of the potential core z_c for the jets at ——— $\mathrm{Re}_D = 5 \times 10^4$ and – – – $\mathrm{Re}_\theta \simeq 480$, and (b) of the peak rms values of velocity u'_z in the entire jets at ——— $\mathrm{Re}_D = 5 \times 10^4$ and – – – $\mathrm{Re}_\theta \simeq 480$, and on the jet axis at ——— $\mathrm{Re}_D = 5 \times 10^4$ and – – – $\mathrm{Re}_\theta \simeq 480$.

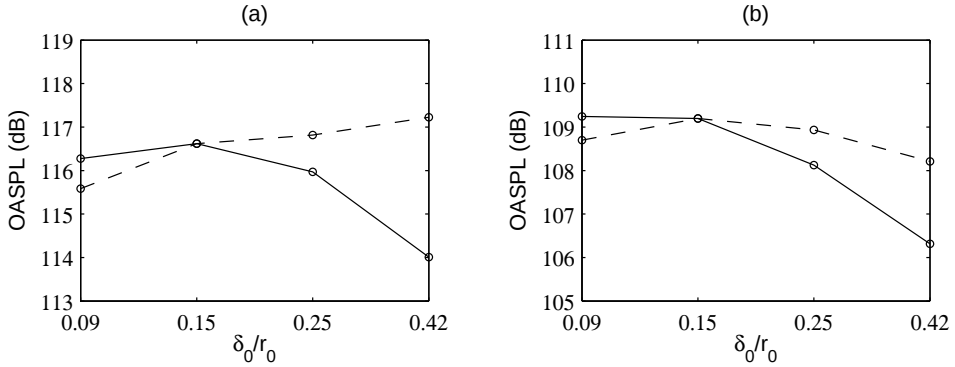

Figure 20. Variations with δ_0/r_0 of the overall sound pressure levels (OASPL) at $60r_0$ from the pipe exit, at the angles ϕ of (a) 40^o and (b) 90^o, for the jets at ——— $\mathrm{Re}_D = 5 \times 10^4$ and – – – $\mathrm{Re}_\theta \simeq 480$.

To briefly conclude, this work demonstrates the importance of the initial shear-layer thickness in subsonic jets with disturbed upstream flow conditions, in terms of both geometry and viscosity effects, induced by the variations of the ratio δ_0/r_0 and of the momentum-thickness Reynolds number Re_θ, respectively. These effects can reinforce or counteract each other, which might render difficult any *a priori* prediction on flow and sound fields. Viscosity effects can nevertheless be expected to dominate in jets at low and moderate Reynolds numbers, but to be rather small in jets at high Reynolds numbers, typically above a threshold value of about $\mathrm{Re}_\theta = 1000$, which should be the case in full-scale industrial jets, but not necessarily in model-scale university jets.

Acknowledgments

This work was granted access to the HPC resources of the Institut du Développement et des Ressources en Informatique Scientifique (IDRIS) under the allocation 2011-020204 made by GENCI (Grand Equipement National de Calcul Intensif).

References

[1]Hussain, A.K.M.F., "Coherent structures–reality and myth," *Phys. Fluids*, Vol. 26, No. 10, 1983, pp. 2816-2850.

[2]Crighton, D.G., "Acoustics as a branch of fluid mechanics," *J. Fluid Mech.*, Vol. 106, 1981, pp. 261-298.

[3]Morris, P.J. and Zaman, K.B.M.Q., "Velocity measurements in jets with application to noise source modelling," *J. Sound Vib.*, Vol. 329, No. 4, 2009, pp. 394-414.

[4]Arakeri, V.H., Krothapalli, A., Siddavaram, V., Alkislar, M.B., and Lourenco, L., "On the use of microjets to suppress turbulence in a Mach 0.9 axisymmetric jet," *J. Fluid Mech.*, Vol. 490, 2003, pp. 75-98.

[5]Crow, S.C. and Champagne, F.H., "Orderly structure in jet turbulence," *J. Fluid Mech.*, Vol. 48, 1971, pp. 547-591.

[6]Zaman, K.B.M.Q., "Effect of initial condition on subsonic jet noise," *AIAA J.*, Vol. 23, 1985, pp. 1370-1373.

[7]Zaman, K.B.M.Q., "Far-field noise of a subsonic jet under controlled excitation," *J. Fluid Mech.*, Vol. 152, 1985, pp. 83-111.

[8]Zaman, K.B.M.Q., "Effect of nozzle exit conditions on subsonic jet noise," *17th AIAA/CEAS Aeroacoustics Conference*, 6-8 June 2011, Portland, Oregon, USA, AIAA 2011-2705.

[9]Deo, R.C., Mi, J., and Nathan, G.J., "The influence of Reynolds number on a plane jet," *Phys. Fluids*, Vol. 20, No. 1, 2008, 075108.

[10]Becker, H.A. and Massaro, T.A., "Vortex evolution in a round jet," *J. Fluid Mech.*, Vol. 31, No.3, 1968, pp. 435-448.

[11]Hasan, M.A.Z. and Hussain, A.K.M.F., "The self-excited axisymmetric jet," *J. Fluid Mech.*, Vol. 115, 1982, pp. 59-80.

[12]Viswanathan, K. and Clark, L.T., "Effect of nozzle internal contour on jet aeroacoustics," *Int. J. of Aeroacoustics*, Vol. 3, No. 2, 2004, pp. 103-135.

[13]Harper-Bourne, M., "Jet noise measurements: past and present," *Int. J. of Aeroacoustics*, Vol. 9, No. 4 & 5, 2010, pp. 559-588.

[14]Bridges, J.E. and Hussain, A.K.M.F., "Roles of initial conditions and vortex pairing in jet noise," *J. Sound Vib.*, Vol. 117, No. 2, 1987, pp. 289-311.

[15]Raman, G., Zaman, K.B.M.Q., and Rice, E.J., "Initial turbulence effect on jet evolution with and without tonal excitation," *Phys. Fluids A*, Vol. 1, No. 7, 1989, pp. 1240-1248.

[16]Hussain, A.K.M.F and Zedan, M.F., "Effects of the initial condition on the axisymmetric free shear layer: Effects of the initial momentum thickness," *Phys. Fluids*, Vol. 21, No. 7, 1978, pp. 1100-1112.

[17]Michalke, A., "Survey on jet instability theory," *Prog. Aerospace Sci.*, Vol. 21, 1984, pp. 159-199.

[18]Cohen, J. and Wygnanski, I., "The evolution of instabilities in the axisymmetric jet. Part 1: the linear growth of disturbances near the nozzle," *J. Fluid Mech.*, Vol. 176, 1987, pp. 191-219.

[19]Morris, P.J., "The spatial viscous instability of axisymmetric jets," *J. Fluid Mech.*, Vol. 77, No. 3, 1976, pp. 511529.

[20]Morris, P.J., "Viscous stability of compressible axisymmetric jets," *AIAA J.*, Vol. 21, No. 4, 1983, pp. 481482.

[21]Gutmark, E. and Ho, C.-M., "Preferred modes and the spreading rates of jets," *Phys. Fluids*, Vol. 26, No. 10, 1983, pp. 2932-2938.

[22]Brown, G.L. and Roshko, A., "Density effect and large structure in turbulent mixing layers," *J. Fluid Mech.*, Vol. 64, 1974, pp. 775816.

[23]Kleinman, R.R. and Freund, J.B., "The sound from mixing layers simulated with different ranges of turbulent scales," *Phys. Fluids*, Vol. 20, No. 10, 2008, 101503.

[24]Bogey, C., Marsden, O. and Bailly, C., "Flow and sound fields of initially tripped jets at Reynolds numbers ranging from 25,000 to 200,000," *50th AIAA Aerospace Sciences Meeting*, 9-12 January 2012, Nashville, TN, USA, AIAA 2012-1172.

[25]Colonius, T. and Lele, S.K., "Computational aeroacoustics: progress on nonlinear problems of sound generation," *Progress in Aerospace Sciences*, Vol. 40, 2004, pp. 345-416.

[26]Bailly, C. and Bogey, C., "Contributions of CAA to jet noise research and prediction," *Int. J. Comput. Fluid Dyn.*, Vol. 18, No. 6, 2004, pp. 481-491.

[27]Wang, M., Freund J.B., and Lele, S.K., "Computational prediction of flow-generated sound," *Annu. Rev. Fluid. Mech.*, Vol. 38, 2006, pp. 483-512.

[28]Stanley, S.A. and Sarkar, S., "Influence of nozzle conditions and discrete forcing on turbulent planar jets," *AIAA J.*, Vol. 38, No. 9, 2000, pp. 1615-1623.

[29]Bogey, C. and Bailly, C., "Effects of inflow conditions and forcing on a Mach 0.9 jet and its radiated noise," *AIAA J.*, Vol. 43, No. 5, 2005, pp. 1000-1007.

[30]Kim, J. and Choi, H., "Large eddy simulation of a circular jet: effect of inflow conditions on the near field," *J. Fluid Mech.*, Vol. 620, 2009, pp. 383-411.

[31]Bogey, C. and Bailly, C., "Influence of nozzle-exit boundary-layer conditions on the flow and acoustic fields of initially laminar jets," *J. Fluid Mech.*, Vol. 663, 2010, pp. 507-539.

[32]Bogey, C., Marsden, O., and Bailly, C., "Large-Eddy Simulation of the flow and acoustic fields of a Reynolds number 10^5 subsonic jet with tripped exit boundary layers," *Phys. Fluids*, Vol. 23, No. 3, 2011, 035104.

[33]Bogey, C., Marsden, O., and Bailly, C., "On the spectra of nozzle-exit velocity disturbances in initially nominally turbulent jets," *Phys. Fluids*, Vol. 23, No. 9, 2011, 091702.

[34]Bogey, C., Marsden, O. and Bailly, C., "Influence of initial turbulence level on the flow and sound fields of a subsonic jet at a diameter-based Reynolds number of 10^5," to appear in *J. Fluid Mech.*, 2012. See also AIAA 2011-2837.

[35]Mohseni, K. and Colonius, T., "Numerical treatment of polar coordinate singularities," *J. Comput. Phys.*, Vol. 157, No. 2, 2000, pp. 787-795.

[36]Bogey, C., de Cacqueray, N., and Bailly, C., "Finite differences for coarse azimuthal discretization and for reduction of effective resolution near origin of cylindrical flow equations," *J. Comput. Phys.*, Vol. 230, No. 4, 2011, pp. 1134-1146.

[37]Bogey, C. and Bailly, C., "A family of low dispersive and low dissipative explicit schemes for flow and noise computations," *J. Comput. Phys.*, Vol. 194, No. 1, 2004, pp. 194-214.

[38]Bogey, C., de Cacqueray, N., and Bailly, C., "A shock-capturing methodology based on adaptative spatial filtering for high-order non-linear computations," *J. Comput. Phys.*, Vol. 228, No. 5, 2009, pp. 1447-1465.

[39]Berland, J., Bogey, C., Marsden, O., and Bailly, C., "High-order, low dispersive and low dissipative explicit schemes for multi-scale and boundary problems," *J. Comput. Phys.*, Vol. 224, No. 2, 2007, pp. 637-662.

[40]Tam, C.K.W and Dong, Z., "Radiation and outflow boundary conditions for direct computation of acoustic and flow disturbances in a nonuniform mean flow., *J. Comput. Acoust.*, Vol. 4, No. 2,, 1996, pp. 175201.

[41]Bogey, C. and Bailly, C., "Three-dimensional non reflective boundary conditions for acoustic simulations: far-field formulation and validation test cases," *Acta Acustica*, Vol. 88, No. 4, 2002, pp. 463-471.

[42]Bogey, C. and Bailly, C., "Large Eddy Simulations of transitional round jets: influence of the Reynolds number on flow development and energy dissipation," *Phys. Fluids*, Vol. 18, No. 6, 2006, 065101.

[43]Bogey, C. and Bailly, C., "Large eddy simulations of round jets using explicit filtering with/without dynamic Smagorinsky model," *Int. J. Heat and Fluid Flow*, Vol. 27, No. 4, 2006, pp. 603-610.

[44]Bogey, C. and Bailly, C., "Turbulence and energy budget in a self-preserving round jet: direct evaluation using large-eddy simulation," *J. Fluid Mech.*, Vol. 627, 2009.

[45]Bogey, C., Barré, S., Juvé, D., and Bailly, C., "Simulation of a hot coaxial jet : direct noise prediction and flow-acoustics correlations," *Phys. Fluids*, Vol. 21, No. 3, 2009, 035105.

[46]Ahuja, K.K., Tester, B.J., and Tanna, H.K., "Calculation of far field jet noise spectra from near field measurements with true source location," *J. Sound Vib.*, Vol. 116, No. 3, 1987, pp. 415-426.

[47]Batt, R.G., "Some measurements on the effect of tripping the two-dimensional shear layer," *AIAA J.*, Vol. 13, No. 2, 1975, pp. 245-247.

[48]Lau, J.C., Morris, P.J., and Fisher, M.J., "Measurements in subsonic and supersonic free jets using a laser velocimeter," *J. Fluid Mech.*, Vol. 93, No. 1, 1979, pp. 1-27.

[49]Fleury, V., Bailly, C., Jondeau, E., Michard, M., and Juvé, D., "Space-time correlations in two subsonic jets using dual-PIV measurements," *AIAA J.*, Vol. 46, No. 10, 2008, pp. 2498-2509.

[50]Mollo-Christensen, E., Kolpin, M.A., and Martucelli, J.R., "Experiments on jet flows and jet noise far-field spectra and directivity patterns," *J. Fluid Mech.*, Vol. 18, No. 2, 1964, pp. 285-301.

[51]Lush, P.A., "Measurements of subsonic jet noise and comparison with theory," *J. Fluid Mech.*, Vol. 46, No. 3, 1971, pp. 477-500.

[52]Bogey, C., Barré, S., Fleury, V., Bailly, C., and Juvé, D., "Experimental study of the spectral properties of near-field and far-field jet noise," *Int. J. of Aeroacoustics*, Vol. 6, No. 2, 2007, pp. 73-92.

[53]Tanna, H.K., "An experimental study of jet noise. Part I: Turbulent mixing noise," *J. Sound Vib.*, Vol. 50, No. 3, 1977, pp. 405-428.

[54]Bogey, C., Bailly, C., and Juvé, D., "Noise investigation of a high subsonic, moderate Reynolds number jet using a compressible LES," *Theoret. Comput. Fluid Dynamics*, Vol. 16, No. 4, 2003, pp. 273-297.

[55]Panda, J., Seasholtz, R.G., and Elam, K.A., "Investigation of noise sources in high-speed jets via correlation measurements," *J. Fluid Mech.*, Vol. 537, 2005, pp. 349-385.

[56]Bogey, C. and Bailly, C., "An analysis of the correlations between the turbulent flow and the sound pressure field of subsonic jets," *J. Fluid Mech.*, Vol. 583, 2007, pp. 71-97.

[57]Tam, C.K.W., Viswanathan, K., Ahuja, K.K., and Panda, J., "The sources of jet noise: experimental evidence," *J. Fluid Mech.*, Vol. 615, 2008, p. 253-292.